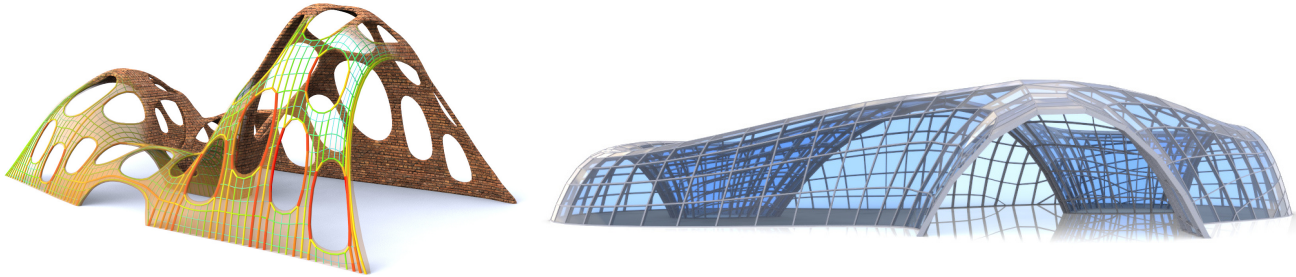


# Design of Self-supporting Surfaces



**Figure 1:** Left: Surfaces with irregularly placed holes are hard to realize as masonry, where the mortar between bricks must not be subject to tensile stresses. The surface shown here has this surprising property – it has been found as the nearest self-supporting shape from a given freeform geometry. The fictitious thrust network used in our algorithms is also shown, with edges' cross-section and coloring visualizing the magnitude of forces (warmer colors represent higher stresses.) Right: Curvature analysis with respect to the so-called Airy stress surface tells us how to remesh shapes by self-supporting quad meshes with planar faces, which guide steel/glass constructions with low moments in nodes.

## 1 Abstract

Self-supporting masonry is one of the most ancient and elegant techniques for building curved shapes. Because of the very geometric nature of their failure, analyzing and modeling such structures is more a geometry processing problem than one of classical continuum mechanics. In this paper we use the thrust network method of analysis and present an iterative nonlinear optimization algorithm for efficiently approximating freeform shapes by self-supporting ones. The rich geometry of thrust networks leads us to close connections between different topics of discrete differential geometry, such as a finite-element discretization of the Airy stress potential, perfect graph Laplacians, and the problem of computing admissible loads via curvatures of polyhedral surfaces. This geometric viewpoint allows us, in particular, to remesh self-supporting shapes by self-supporting quad meshes with planar faces. This leads to another application of the theory: steel/glass constructions with low moments in nodes.

**CR Categories:** I.3.5 [Computer Graphics]: Computational Geometry and Object Modeling—Curve, surface, solid, and object representations;

**Keywords:** Discrete differential geometry, architectural geometry, self-supporting masonry, thrust networks, reciprocal force diagrams, discrete Laplace operators, isotropic geometry, mean curvature

## 1 Introduction

Vaulted masonry structures are among the simplest and at the same time most elegant solutions for creating curved shapes in building construction. For this reason they have been an object of interest since antiquity; large, non-convex examples of such structures include gothic cathedrals. They continue to be an active topic of research today.

Our paper is concerned with a combined geometry+statics analysis of *self-supporting* masonry and with tools for the interactive modeling of freeform self-supporting structures. Here “self-supporting” means that the structure, considered as an arrangement of blocks

(bricks, stones), holds together by itself, with additional support present only during construction. This analysis is based on the following assumptions, which follow the classic [Heyman 1966]:

**Assumption 1:** Masonry has no tensile strength, but the individual building blocks do not slip against each other (because of friction or mortar). On the other hand, their compressive strength is sufficiently high so that failure of the structure is by a sudden change in geometry and not by material failure.

**Assumption 2 (The Safe Theorem):** If a system of forces can be found which is in equilibrium with the load on the structure and which is contained within the masonry envelope then the structure will carry the loads, although the actual forces present may not be those postulated by that system.

Our approach is twofold: We first give an overview of the continuous case of a smooth surface under stress, which turns out to be governed locally by the so-called Airy stress function. This mathematical model is called a membrane in the engineering literature and has been applied to the analysis of masonry before. The surface is self-supporting if and only if stresses are entirely compressive. For computational purposes, stresses are discretized as a fictitious *thrust network* [Block and Ochsendorf 2007] contained in the masonry structure; this network is a system of forces in equilibrium with the structure’s deadload. It can be interpreted as a finite element discretization of the continuous case, and it turns out to have very interesting geometry, with the Airy stress function becoming a polyhedral surface directly related to a reciprocal force diagram.

While previous work in architectural geometry was mostly concerned with aspects of rationalization and purely geometric side-conditions which occur in freeform architecture, the focus of this paper is design with *statics* constraints. In particular, our contributions are the following:

### Contributions.

- We present an optimization algorithm, based on the theory of thrust networks and Airy potentials, for efficiently finding a self-supporting surface near a given arbitrary reference surface (§3), and build a tool for interactive design of self-supporting surfaces based on this algorithm (§4). Freeform masonry is based on such surfaces.
- The discrete “stress Laplacian” derived from a thrust network

74 with compressive forces is a so-called perfect one (§2.2). We use it  
 75 to argue why our discretizations are faithful to the continuous case.

- 76 • We connect the physics of self-supporting surfaces with the ge-  
 77 ometry of isotropic 3-space, and express the equations governing  
 78 self-supporting surfaces in terms of curvatures (§2.3) and (§2.4).  
 79 Likewise we establish a connection between the stress Laplacian  
 80 and mean curvatures of polyhedral surfaces. This theoretical part  
 81 of the paper is a contribution to Discrete Differential Geometry.  
 82
- We use the geometric knowledge we have gathered to find par-  
 83 ticularly nice families of self-supporting surfaces, especially planar  
 84 quadrilateral representations of thrust networks (§5). This leads to  
 85 steel/glass structures with low bending and torsion moments.

86 **Related Work.** Unsupported masonry has been an active topic of  
 87 research in the engineering community. The foundations for the  
 88 modern approach were laid by Jacques Heyman [1966] and are  
 89 available as the textbook [Heyman 1995]. The theory of reciprocal  
 90 force diagrams in the planar case was studied by Maxwell [Maxwell  
 91 1864]; a unifying view on polyhedral surfaces, compressive forces  
 92 and corresponding “convex” force diagrams is presented by [Ash  
 93 et al. 1988]. F. Fraternali [2002], [2010] established a connection  
 94 between the continuous theory of stresses in membranes and the  
 95 discrete theory of forces in thrust networks, by interpreting the lat-  
 96 ter as a non-conforming finite element discretization of the former.

97 Several authors have studied the problem of finding discrete com-  
 98 pressive force networks contained within the boundary of masonry  
 99 structures; previous work in this area includes [O’Dwyer 1998] and  
 100 [Andreu et al. 2007]. Fraternali [2010] proposed solving for the  
 101 structure’s discrete stress surface, and examining its convex hull to  
 102 study the structure’s stability and susceptibility to cracking.

103 Philippe Block’s seminal thesis introduced *Thrust Network Analy-  
 104 sis*, which pioneered the use of thrust networks and their reciprocal  
 105 diagrams for efficient and practical design of self-supporting  
 106 masonry structures. By first seeking a reciprocal diagram of the top  
 107 view, guaranteeing equilibrium of horizontal forces, then solving  
 108 for the heights that balance the vertical loads, Thrust Network Analy-  
 109 sis linearizes the form-finding problem. For a thorough overview  
 110 of this methodology, see e.g. [Block and Ochsendorf 2007; Block  
 111 2009]. Recent work by Block and coauthors extends this method  
 112 in the case where the reciprocal diagram is not unique; for different  
 113 choices of reciprocal diagram, the optimal heights can be found us-  
 114 ing the method of least squares [Van Mele and Block 2011], and the  
 115 search for the best such reciprocal diagram can be automated using  
 116 a genetic algorithm [Block and Lachauer 2011].

117 Other approaches to the interactive design of self-supporting struc-  
 118 tures include modeling these structures as damped particle-spring  
 119 systems [Kilian and Ochsendorf 2005; Barnes 2009], and mirroring  
 120 the rich tradition in architecture of designing self-supporting  
 121 surfaces using hanging chain models [Heyman 1998]. Alterna-  
 122 tively, masonry structures can be represented by networks of rigid  
 123 blocks [Livesley 1992], whose conditions on the structural feasibil-  
 124 ity were incorporated into procedural modeling of buildings [Whit-  
 125 ing et al. 2009].

126 Algorithmic and mathematical methods relevant to this paper are  
 127 work on the geometry of quad meshes with planar faces [Glymph  
 128 et al. 2004; Liu et al. 2006], discrete curvatures for such meshes  
 129 [Pottmann et al. 2007; Bobenko et al. 2010], in particular curva-  
 130 tures in isotropic geometry [Pottmann and Liu 2007]. Schiftner and  
 131 Balzer [2010] discuss approximating a reference surface by a quad  
 132 mesh with planar faces, whose layout is guided by statics properties  
 133 of that surface.

## 134 2 Self-supporting Surfaces

135 This section is the theoretical basis of the paper. §2.1 and §2.2 ex-  
 136 plain the mathematical model for unsupported masonry and its dis-  
 137 cretization, which is needed in our modeling algorithms. The con-  
 138 nection with isotropic geometry (§2.3 and §2.4) is important for the  
 139 later Section 5, which deals with self-supporting PQ meshes and  
 140 moment-free steel/glass constructions.

### 141 2.1 The Continuous Theory

142 We model masonry as a surface given by a height field  $s(x, y)$  de-  
 143 fined in some planar domain  $\Omega$ . We assume that there are vertical  
 144 loads  $F(x, y)$  — usually  $F$  represents the structure’s own weight.  
 145 By definition this surface is self-supporting if and only if there ex-  
 146 ists a field of compressive stresses which are in equilibrium with  
 147 the acting forces. This is equivalent to existence of a field  $M(x, y)$   
 148 of  $2 \times 2$  symmetric positive semidefinite matrices satisfying

$$\text{div}(M\nabla s) = F, \quad \text{div } M = 0, \quad (1)$$

149 where the divergence operator  $\text{div} \begin{pmatrix} u(x,y) \\ v(x,y) \end{pmatrix} = u_x + v_y$  is under-  
 150 stood to act on the columns of a matrix (see e.g. [Fraternali 2010],  
 151 [Giaquinta and Giusti 1985]).

152 The condition  $\text{div } M = 0$  says that  $M$  is locally the Hessian of a  
 153 real-valued function  $\phi$  (the *Airy stress potential*): With the notation

$$M = \begin{pmatrix} m_{11} & m_{12} \\ m_{12} & m_{22} \end{pmatrix} \iff \widehat{M} = \begin{pmatrix} m_{22} & -m_{12} \\ -m_{12} & m_{11} \end{pmatrix}$$

154 it is clear that  $\text{div } M = 0$  is an integrability condition for  $\widehat{M}$ , so  
 155 locally there is a potential  $\phi$  with

$$\widehat{M} = \nabla^2 \phi, \quad \text{i.e.,} \quad M = \widehat{\nabla^2 \phi}.$$

156 If the domain  $\Omega$  is simply connected, this relation holds globally.  
 157 Positive semidefiniteness of  $M$  (or equivalently of  $\widehat{M}$ ) character-  
 158 izes *convexity* of the Airy potential  $\phi$ . The Airy function enters  
 159 computations only by way of its derivatives, so global existence is  
 160 not an issue.

161 *Remark:* Stresses at boundary points depend on the way the sur-  
 162 face is anchored: A fixed anchor means no condition, but a free  
 163 boundary with outer normal vector  $\mathbf{n}$  means  $\langle M\nabla s, \mathbf{n} \rangle = 0$ .

164 **Stress Laplacian.** Note that  $\text{div } M = 0$  yields  $\text{div}(M\nabla s) =$   
 165  $\text{tr}(M\nabla^2 s)$ , which we like to call  $\Delta_\phi s$ . The operator  $\Delta_\phi$  is sym-  
 166 metric. It is elliptic (as a Laplace operator should be) if and only if  
 167  $M$  is positive definite, i.e.,  $\phi$  is strictly convex. The balance condi-  
 168 tion (1) may be written as  $\Delta_\phi s = F$ .

### 169 2.2 Discrete Theory: Thrust Networks

170 We discretize a self-supporting surface by a mesh  $\mathcal{S} = (V, E, F)$   
 171 (see Figure 2). Loads are again vertical, and we discretize them as  
 172 force densities  $F_i$  associated with vertices  $\mathbf{v}_i$ . The load acting on  
 173 this vertex is then given by  $F_i A_i$ , where  $A_i$  is an area of influence  
 174 (using a prime to indicate projection onto the  $xy$  plane,  $A_i$  is the  
 175 area of the Voronoi cell of  $\mathbf{v}'_i$  w.r.t.  $V'$ ). We assume that stresses  
 176 are carried by the edges of the mesh: the force exerted on the vertex  
 177  $\mathbf{v}_i$  by the edge connecting  $\mathbf{v}_i, \mathbf{v}_j$  is given by

$$w_{ij}(\mathbf{v}_j - \mathbf{v}_i), \quad \text{where} \quad w_{ij} = w_{ji} \geq 0.$$

178 The nonnegativity of the individual weights  $w_{ij}$  expresses the com-  
 179 pressive nature of forces. The balance conditions at vertices then

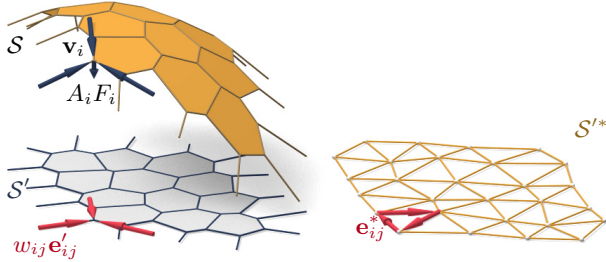


**Figure 2:** A thrust network  $\mathcal{S}$  with dangling edges indicating external forces (left). This network together with compressive forces which balance vertical loads  $A_i F_i$  projects onto a planar mesh  $\mathcal{S}'$  with equilibrium compressive forces  $w_{ij} \mathbf{e}'_{ij}$  in its edges. Rotating forces by  $90^\circ$  leads to the reciprocal force diagram  $\mathcal{S}'^*$  (right).

180 read as follows: With  $\mathbf{v}_i = (x_i, y_i, s_i)$  we have

$$\sum_{j \sim i} w_{ij}(x_j - x_i) = \sum_{j \sim i} w_{ij}(y_j - y_i) = 0, \quad (2)$$

$$\sum_{j \sim i} w_{ij}(s_j - s_i) = A_i F_i. \quad (3)$$

181 A mesh equipped with edge weights in this way is a discrete *thrust* 182 network. Invoking the safe theorem, we can state that a masonry 183 structure is self-supporting, if we can find a thrust network with 184 compressive forces which is entirely contained within the structure.

185 **Reciprocal Diagram.** Equations (2) have a geometric interpretation: 186 with edge vectors

$$\mathbf{e}'_{ij} = \mathbf{v}'_j - \mathbf{v}'_i = (x_j, y_j) - (x_i, y_i),$$

187 Equation (2) asserts that vectors  $w_{ij} \mathbf{e}'_{ij}$  form a closed cycle. Rotating 188 them by 90 degrees, we see that likewise

$$\mathbf{e}'^*_{ij} = w_{ij} J \mathbf{e}'_{ij}, \quad \text{with } J = \begin{pmatrix} 0 & -1 \\ 1 & 0 \end{pmatrix},$$

189 form a closed cycle (see Figure 2). If the mesh  $\mathcal{S}$  is simply connected, 190 there exists an entire *reciprocal diagram*  $\mathcal{S}'^*$  which is a 191 combinatorial dual of  $\mathcal{S}$ , and which has edge vectors  $\mathbf{e}'^*_{ij}$ . Its 192 vertices are denoted by  $\mathbf{v}'^*_i$ .

193 *Remark:* If  $\mathcal{S}'$  is a Delaunay triangulation, then the corresponding 194 Voronoi diagram is an example of a reciprocal diagram.

195 **Polyhedral Stress Potential.** We can go further and construct a 196 convex polyhedral “Airy stress potential” surface  $\Phi$  with vertices 197  $\mathbf{w}_i = (x_i, y_i, \phi_i)$  combinatorially equivalent to  $\mathcal{S}$  by requiring that 198 a primal face of  $\Phi$  lies in the plane  $z = \alpha x + \beta y + \gamma$  if and only if 199  $(\alpha, \beta)$  is the corresponding dual vertex of  $\mathcal{S}'^*$  (see Figure 3). Ob- 200 viously this condition determines  $\Phi$  up to vertical translation. For 201 existence see [Ash et al. 1988]. The inverse procedure constructs 202 a reciprocal diagram from  $\Phi$ . This procedure works also if forces 203 are not compressive: we can construct an Airy mesh  $\Phi$  which has 204 planar faces, but it will no longer be a convex polyhedron.

205 The vertices of  $\Phi$  can be interpolated by a piecewise-linear function 206  $\phi(x, y)$ . It is easy to see that the derivative of  $\phi(x, y)$  jumps by the 207 amount  $\|\mathbf{e}'^*_{ij}\| = w_{ij} \|\mathbf{e}'_{ij}\|$  when crossing over the edge  $\mathbf{e}'_{ij}$  at right 208 angle, with unit speed. This identifies  $\Phi$  as the Airy polyhedron in- 209 troduced by [Fraternali et al. 2002] as a finite element discretization 210 of the continuous Airy function (see also [Fraternali 2010]).

211 If the mesh is not simply connected, the reciprocal diagram and 212 the Airy polyhedron exist only locally. Our computations do not 213 require global existence.

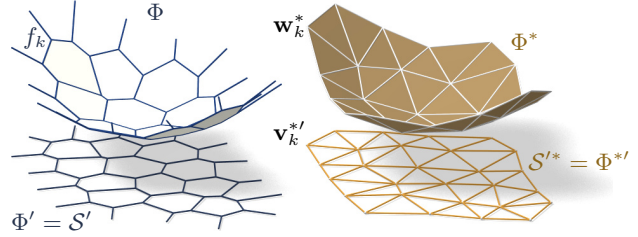


**Figure 3:** Airy stress potential  $\Phi$  and its polar dual  $\Phi^*$ .  $\Phi$  projects onto the same planar mesh as  $\mathcal{S}$  does, while  $\Phi^*$  projects onto the reciprocal force diagram. A primal face  $f_k$  lies in the plane  $z = \alpha x + \beta y + \gamma \iff$  the corresponding dual vertex is  $\mathbf{w}_k^* = (\alpha, \beta, -\gamma)$ .

214 **Polarity.** Polarity with respect to the *Maxwell paraboloid*  $z =$   
215  $\frac{1}{2}(x^2 + y^2)$  maps the plane  $z = \alpha x + \beta y + \gamma$  to the point  $(\alpha, \beta, -\gamma)$ .  
216 Thus, applying polarity to  $\Phi$  and projecting the result  $\Phi^*$  into the  $xy$   
217 plane reconstructs the reciprocal diagram  $\Phi'^* = \mathcal{S}'^*$  (see Fig. 3).

218 **Discrete Stress Laplacian.** The weights  $w_{ij}$  may be used to de-  
219 fine a graph Laplacian  $\Delta_\phi$  which on vertex-based functions acts as

$$\Delta_\phi s(\mathbf{v}_i) = \sum_{j \sim i} w_{ij}(s_j - s_i).$$

220 This operator is a perfect discrete Laplacian in the sense of [War-  
221 detzky et al. 2007], since it is symmetric by construction, Equa-  
222 tion (2) implies linear precision for the planar “top view mesh”  $\mathcal{S}'$   
223 (i.e.,  $\Delta_\phi f = 0$  if  $f$  is a linear function), and  $w_{ij} \geq 0$  ensures  
224 semidefiniteness and a maximum principle for  $\Delta_\phi$ -harmonic func-  
225 tions. Equation (3) can be written as  $\Delta_\phi s = AF$ .

226 Note that  $\Delta_\phi$  is well defined even when the underlying meshes are  
227 not simply connected.

### 228 2.3 Surfaces in Isotropic Geometry

229 It is worthwhile to reconsider the basics of self-supporting surfaces  
230 in the language of dual-isotropic geometry, which takes place in  $\mathbb{R}^3$   
231 with the  $z$  axis as a distinguished vertical direction. The basic ele-  
232 ments of this geometry are planes, having equation  $z = f(x, y) =$   
233  $\alpha x + \beta y + \gamma$ . The gradient vector  $\nabla f = (\alpha, \beta)$  determines the  
234 plane up to translation. A plane tangent to the graph of the function  
235  $s(x, y)$  has gradient vector  $\nabla s$ .

236 There is the notion of *parallel points*:  $(x, y, z) \parallel (x', y', z') \iff$   
237  $x = x', y = y'$ .

238 *Remark:* The Maxwell paraboloid is considered the unit sphere of  
239 isotropic geometry, and the geometric quantities considered above  
240 are assigned specific meanings: The forces  $\|\mathbf{e}'^*_{ij}\| = w_{ij} \|\mathbf{e}'_{ij}\|$  are  
241 dihedral angles of the Airy polyhedron  $\Phi$ , and also “lengths” of  
242 edges of  $\Phi^*$ . We do not use this terminology in the sequel.

243 **Curvatures.** Generally speaking, in the differential geometry of  
244 surfaces one considers the *Gauss map*  $\sigma$  from a surface  $S$  to a con-  
245 vex unit sphere  $\Phi$  by requiring that corresponding points have par-  
246 allel tangent planes. Subsequently mean curvature  $H^{\text{rel}}$  and Gaus-  
247 sian curvature  $K^{\text{rel}}$  relative to  $\Phi$  are computed from the derivative  
248  $d\sigma$ . Classically  $\Phi$  is the ordinary unit sphere  $x^2 + y^2 + z^2 = 1$ , so  
249 that  $\sigma$  maps each point to its unit normal vector.

250 In our setting, parallelity is a property of *points* rather than planes,  
251 and the Gauss map  $\sigma$  goes the other way, mapping the tangent

planes of the unit sphere  $z = \phi(x, y)$  to the corresponding tangent plane of the surface  $z = s(x, y)$ . If we know which point a plane is attached to, then the Gauss map is determined by the plane's gradient. So we simply write

$$\nabla\phi \xrightarrow{\sigma} \nabla s.$$

By moving along a curve  $\mathbf{u}(t) = (x(t), y(t))$  in the parameter domain we get the first variation of tangent planes:  $\frac{d}{dt}\nabla\phi|_{\mathbf{u}(t)} = (\nabla^2\phi)\dot{\mathbf{u}}$ . This yields the derivative  $(\nabla^2\phi)\dot{\mathbf{u}} \xrightarrow{d\sigma} (\nabla^2s)\dot{\mathbf{u}}$ , for all  $\dot{\mathbf{u}}$ , and the matrix of  $d\sigma$  is found as  $(\nabla^2\phi)^{-1}(\nabla^2s)$ . By definition, curvatures of the surface  $s$  relative to  $\phi$  are found as

$$K_s^{\text{rel}} = \det(d\sigma) = \frac{\det\nabla^2s}{\det\nabla^2\phi},$$

$$H_s^{\text{rel}} = \frac{1}{2}\text{tr}(d\sigma) = \frac{1}{2}\text{tr}\left(\frac{M}{\det\nabla^2\phi}\nabla^2s\right) = \frac{\Delta_\phi s}{2\det\nabla^2\phi}.$$

The Maxwell paraboloid  $\phi_0(x, y) = \frac{1}{2}(x^2 + y^2)$  is the canonical unit sphere of isotropic geometry, with Hessian  $E_2$ . Curvatures relative to  $\phi_0$  are not called "relative" and are denoted by the symbols  $H, K$  instead of  $H^{\text{rel}}, K^{\text{rel}}$ . The observation

$$\Delta_\phi\phi = \text{tr}(M\nabla^2\phi) = \text{tr}(\widehat{\nabla^2\phi}\nabla^2\phi) = 2\det\nabla^2\phi$$

together with the formulas above implies

$$K_s = \det\nabla^2s, K_\phi = \det\nabla^2\phi \implies H_s^{\text{rel}} = \frac{\Delta_\phi s}{2K_\phi} = \frac{\Delta_\phi s}{\Delta_\phi\phi}.$$

**Relation to Self-supporting Surfaces.** Summarizing the formulas above, we rewrite the balance condition (1) as

$$2K_\phi H_s^{\text{rel}} = \Delta_\phi s = F. \quad (4)$$

Let us draw some conclusions:

- Since  $H_\phi^{\text{rel}} = 1$  we see that the load  $F_\phi = 2K_\phi$  is admissible for the stress surface  $\phi(x, y)$ , which is hereby shown as self-supporting. The quotient of loads yields  $H_s^{\text{rel}} = F/F_\phi$ .
- If the stress surface coincides with the Maxwell paraboloid, then *constant loads characterize constant mean curvature surfaces*, because we get  $K_\phi = 1$  and  $H_s = F/2$ .
- If  $s_1, s_2$  have the same stress potential  $\phi$ , then  $H_{s_1-s_2}^{\text{rel}} = H_{s_1}^{\text{rel}} - H_{s_2}^{\text{rel}} = 0$ , so  $s_1 - s_2$  is a (relative) minimal surface.

## 2.4 Meshes in Isotropic Geometry

A general theory of curvatures of polyhedral surfaces with respect to a polyhedral unit sphere was proposed by [Pottmann et al. 2007; Bobenko et al. 2010], and its dual complement in isotropic geometry was elaborated on in [Pottmann and Liu 2007]. As illustrated by Figure 4, the mean curvature of a self-supporting surface  $\mathcal{S}$  relative to its discrete Airy stress potential is associated with the vertices of  $\mathcal{S}$ . It is computed from areas and mixed areas of faces in the polar polyhedra  $\mathcal{S}^*$  and  $\Phi^*$ :

$$H^{\text{rel}}(\mathbf{v}_i) = \frac{A_i(\mathcal{S}, \Phi)}{A_i(\Phi, \Phi)}, \quad \text{where}$$

$$A_i(\mathcal{S}, \Phi) = \frac{1}{4} \sum_{k: f_k \in 1\text{-ring}(\mathbf{v}_i)} \det(\mathbf{v}'_k, \mathbf{w}'_{k+1}) + \det(\mathbf{w}'_k, \mathbf{v}'_{k+1}).$$

The prime denotes the projection into the  $xy$  plane, and summation is over those dual vertices which are adjacent to  $\mathbf{v}_i$ . Replacing  $\mathbf{v}'_k$  by  $\mathbf{w}'_k$  yields  $A_i(\Phi, \Phi) = \frac{1}{2} \sum \det(\mathbf{w}'_k, \mathbf{w}'_{k+1})$ .

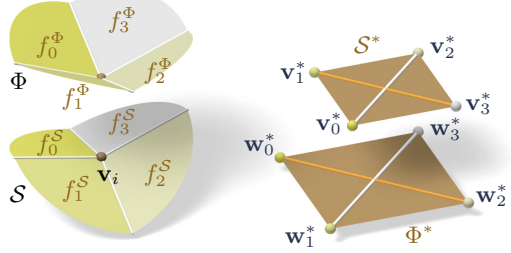


**Figure 4:** Mean curvature of a vertex  $\mathbf{v}_i$  of  $\mathcal{S}$ : Corresponding edges of the polar duals  $\mathcal{S}^*$ ,  $\Phi^*$  are parallel, and mean curvature according to [Pottmann et al. 2007] is computed from the vertices polar to faces adjacent to  $\mathbf{v}_i$ . For valence 4 vertices the case of zero mean curvature shown here is characterized by parallelity of non-corresponding diagonals of corresponding quads in  $\mathcal{S}^*$ ,  $\Phi^*$ .

**Proposition.** If  $\Phi$  is the Airy surface of a thrust network  $\mathcal{S}$ , then the mean curvature of  $\mathcal{S}$  relative to  $\Phi$  is computable as

$$H^{\text{rel}}(\mathbf{v}_i) = \frac{\sum_{j \sim i} w_{ij}(s_j - s_i)}{\sum_{j \sim i} w_{ij}(\phi_j - \phi_i)} = \frac{\Delta_\phi s}{\Delta_\phi\phi}|_{\mathbf{v}_i}. \quad (5)$$

**Proof.** It is sufficient to show  $2A_i(\mathcal{S}, \Phi) = \sum_{j \sim i} w_{ij}(s_j - s_i)$ .

For that, consider edges  $\mathbf{e}'_1, \dots, \mathbf{e}'_n$  emanating from  $\mathbf{v}'_i$ . The dual cycles in  $\Phi^*$  and  $\mathcal{S}^*$  without loss of generality are given by vertices  $(\mathbf{v}'_1, \dots, \mathbf{v}'_n)$  and  $(\mathbf{w}'_1, \dots, \mathbf{w}'_n)$ , respectively. The latter has edges  $\mathbf{w}'_{j+1} - \mathbf{w}'_j = w_{ij}J\mathbf{e}'_j$  (indices modulo  $n$ ).

Without loss of generality  $\mathbf{v}_i = 0$ , so the vertex  $\mathbf{v}'_j$  by construction equals the gradient of the linear function  $\mathbf{x} \mapsto \langle \mathbf{v}'_j, \mathbf{x} \rangle$  defined by the properties  $\mathbf{e}'_{j-1} \mapsto s_{j-1} - s_i$ ,  $\mathbf{e}'_j \mapsto s_j - s_i$ . Corresponding edge vectors  $\mathbf{v}'_{j+1} - \mathbf{v}'_j$  and  $\mathbf{w}'_{j+1} - \mathbf{w}'_j$  are parallel, because  $\langle \mathbf{v}'_{j+1} - \mathbf{v}'_j, \mathbf{e}'_j \rangle = (s_j - s_i) - (s_j - s_i) = 0$ . Expand  $2A_i(\mathcal{S}, \Phi)$ :

$$\begin{aligned} & \frac{1}{2} \sum \det(\mathbf{w}'_j, \mathbf{v}'_{j+1}) + \det(\mathbf{v}'_j, \mathbf{w}'_{j+1}) \\ &= \frac{1}{2} \sum \det(\mathbf{w}'_j - \mathbf{w}'_{j+1}, \mathbf{v}'_{j+1}) + \det(\mathbf{v}'_j, \mathbf{w}'_{j+1} - \mathbf{w}'_j) \\ &= \frac{1}{2} \sum \det(-w_{ij}J\mathbf{e}'_j, \mathbf{v}'_{j+1}) + \det(\mathbf{v}'_j, w_{ij}J\mathbf{e}'_j) \\ &= \sum \det(\mathbf{v}'_j, w_{ij}J\mathbf{e}'_j) = \sum w_{ij} \langle \mathbf{v}'_j, \mathbf{e}'_j \rangle = \sum w_{ij}(s_j - s_i). \end{aligned}$$

Here we have used  $\det(\mathbf{a}, J\mathbf{b}) = \langle \mathbf{a}, \mathbf{b} \rangle$ .  $\square$

In order to discretize (4), we also need a discrete Gaussian curvature, usually defined as a quotient of areas which correspond under the Gauss mapping. We define

$$K_\Phi(\mathbf{v}_i) = \frac{A_i(\Phi, \Phi)}{A_i},$$

where  $A_i$  is the Voronoi area of vertex  $\mathbf{v}'_i$  in the projected mesh  $\mathcal{S}'$  used in (3).

**Remark:** If the faces of the thrust network  $\mathcal{S}$  are not planar, the simple trick of introducing additional edges with zero forces in them makes them planar, and the theory is applicable. In the interest of space, we refrain from elaborating further.

**Discrete Balance Equation.** The discrete version of the balance equation (4) reads as follows:

**Theorem.** A simply-connected mesh  $\mathcal{S}$  with vertices  $\mathbf{v}_i = (x_i, y_i, s_i)$  can be put into static equilibrium with vertical nodal forces  $A_i F_i$  if and only if there exists a combinatorially equivalent

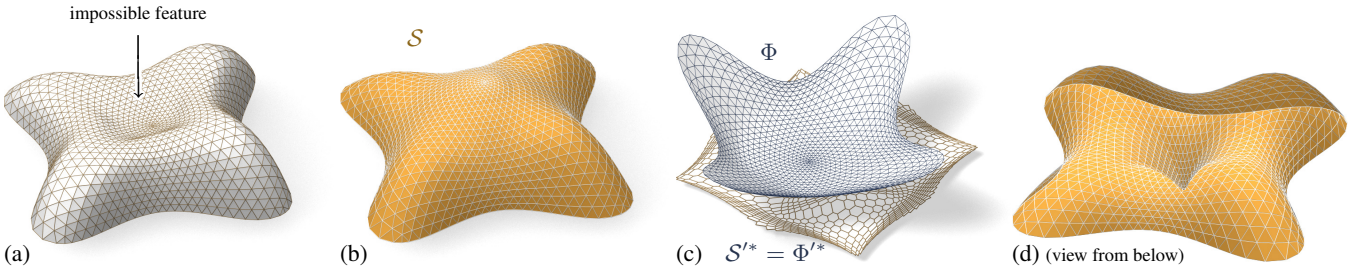


**Figure 5:** The top of the Lilium Tower (a) cannot stand as a masonry structure, because its central part is concave. Our algorithm finds a nearby self-supporting mesh (b) without this impossible feature. (c) shows the corresponding Airy mesh  $\Phi$  and reciprocal force diagram  $S'^*$ . (d) The user can edit the original surface, such as by specifying that the center of the surface is supported by a vertical pillar, and the self-supporting network adjusts accordingly.

316 mesh  $\Phi$  with planar faces and vertices  $(x_i, y_i, \phi_i)$ , such that cur-  
317 vatures of  $\mathcal{S}$  relative to  $\Phi$  obey

$$318 \quad 2K_\Phi(\mathbf{v}_i)H^{\text{rel}}(\mathbf{v}_i) = F_i \quad (6)$$

318 at every interior vertex and every free boundary vertex  $\mathbf{v}_i$ .  $\mathcal{S}$  can  
319 be put into compressive static equilibrium if and only if there exists  
320 a convex such  $\Phi$ .

321 **Proof.** The relation between equilibrium forces  $w_{ij}\mathbf{e}_{ij}$  in  $\mathcal{S}$  and  
322 the polyhedral stress potential  $\Phi$  has been discussed above, and  
323 so has the equivalence “ $w_{ij} \geq 0 \iff \Phi$  convex” (see e.g.  
324 [Ash et al. 1988] for a survey of this and related results). It re-  
325 mains to show that Equations (2) and (6) are equivalent. This is  
326 the case because the proposition above implies  $2K(\mathbf{v}_i)H^{\text{rel}}(\mathbf{v}_i) =$   
327  $2\frac{A_i(\Phi, \Phi)}{A_i} \frac{A_i(\Phi, \mathcal{S})}{A_i(\Phi, \Phi)} = \frac{1}{A_i} (\sum_{j \sim i} w_{ij} (s_j - s_i)) = \frac{1}{A_i} A_i F_i$ .  $\square$

328 **Existence of Discretizations.** When considering discrete thrust  
329 networks as discretizations of continuous self-supporting surfaces,  
330 the following question is important: For a given smooth surface  
331  $s(x, y)$  with Airy stress function  $\phi$ , does there exist a polyhedral  
332 surface  $\mathcal{S}$  in equilibrium approximating  $s(x, y)$ , whose top view  
333 is a given planar mesh  $\mathcal{S}'$ ? We restrict our attention to triangle  
334 meshes, where planarity of the faces of the discrete stress surface  $\Phi$   
335 is not an issue. This question has several equivalent reformulations:

- 336 • Does  $\mathcal{S}'$  have a reciprocal diagram whose corresponding Airy  
337 polyhedron  $\Phi$  approximates the continuous Airy potential  $\phi$ ?  
338 (if the surfaces involved are not simply connected, these ob-  
339 jects are defined locally).
- 340 • Does  $\mathcal{S}'$  possess a “perfect” discrete Laplace-Beltrami oper-  
341 ator  $\Delta_\phi$  in the sense of Wardetzky et al. [2007] whose weights  
342 are the edge length scalars of such a reciprocal diagram?

343 From [Wardetzky et al. 2007] we know that perfect Laplacians ex-  
344 ist only on regular triangulations which are projections of convex  
345 polyhedra. On the other hand, previous sections show how to ap-  
346 propriately re-triangulate: Let  $\Phi$  be a triangle mesh convex hull of  
347 the vertices  $(x_i, y_i, \phi(x_i, y_i))$ , where  $(x_i, y_i)$  are vertices of  $\mathcal{S}'$ .  
348 Then its polar dual  $\Phi^*$  projects onto a reciprocal diagram with pos-  
349 itive edge weights, so  $\Delta_\phi$  has positive weights, and the vertices  
350  $(x_i, y_i, s_i)$  of  $\mathcal{S}$  can be found by solving the discrete Poisson prob-  
351 lem  $(\Delta_\phi s)_i = A_i F_i$ .

352 Assuming the discrete  $\Delta_\phi$  approximates its continuous counter-  
353 part, this yields a mesh approximating  $s(x, y)$ , and we conclude: A  
354 *smooth self-supporting surface can be approximated by a discrete*  
355 *self-supporting triangular mesh for any sampling of the surface.*

### 3 Thrust Networks from Reference Meshes

357 Consider now the problem of taking a given reference mesh, say  
358  $\mathcal{R}$ , and finding a combinatorially equivalent mesh  $\mathcal{S}$  in static equi-  
359 librium approximating  $\mathcal{R}$ . The loads on  $\mathcal{S}$  include user-prescribed  
360 loads as well as the dead load caused by the mesh’s own weight.  
361 Conceptually, finding  $\mathcal{S}$  amounts to minimizing some formulation  
362 of distance between  $\mathcal{R}$  and  $\mathcal{S}$ , subject to constraints (2), (3), and  
363  $w_{ij} \geq 0$ . For any choice of distance this minimization will be a  
364 nonlinear, non-convex, inequality-constrained variational problem.  
365 Our experience with black-box solvers [Wächter and Biegler 2006]  
366 is that they perform well for surfaces without complex geometry or  
367 for polishing reference meshes close to self-supporting, but fail to  
368 converge in reasonable time for more complicated shapes such as  
369 the one of Fig. 1, left. We therefore propose the following special-  
370 ized, staggered linearization for solving the optimization problem:

- 371 0. Start with an initial guess  $\mathcal{S} = \mathcal{R}$ .
- 372 1. Estimate the self-load on the vertices of  $\mathcal{S}$ , using their current  
373 positions.
- 374 2. Fixing  $\mathcal{S}$ , locally fit an associated stress surface  $\Phi$ .
- 375 3. Alter positions  $\mathbf{v}_i$  to improve the fit.
- 376 4. Repeat from Step 1 until convergence.

377 **Remark:** This staggered approach shares the several advantages of  
378 solving the full nonlinear problem: a nearby self-supporting surface  
379 is found given only a suggested reference shape, without needing  
380 to single one of the many possible top view reciprocal diagrams or  
381 needing to specify boundary tractions – these are found automati-  
382 cally during optimization. Although providing an initial top view  
383 graph with good combinatorics remains important, by not fixing the  
384 top view our approach allows the thrust network to slide both ver-  
385 tically and tangentially to the ground, essential to finding faithful  
386 thrust networks for surfaces with free boundary conditions.

387 **Step 1: Estimating Self-Load.** The dead load due to the sur-  
388 face’s own weight depends not only on the top view of  $\mathcal{S}$ , but also  
389 on the surface area of its faces. To avoid adding nonlinearity to  
390 the algorithm, we estimate the load coefficients  $F_i$  at the beginning  
391 of each iteration, and assume they remain constant until the next  
392 iteration. We estimate the load  $A_i F_i$  associated with each vertex  
393 by calculating its Voronoi surface area on each of its incident faces  
394 (note that this surface area is distinct from  $A_i$ , the vertex’s Voronoi  
395 area on the top view), and then multiplying by a user-specified sur-  
396 face density  $\rho$ .

397 **Step 2: Fit a Stress Surface.** In this step, we fix  $\mathcal{S}$  and try to  
398 fit a stress surface  $\Phi$  subordinate to the top view  $\mathcal{S}'$  of the primal  
399 mesh. We do so by searching for dihedral angles between the faces  
400 of  $\Phi$  which minimize, in the least-squares sense, the error in force

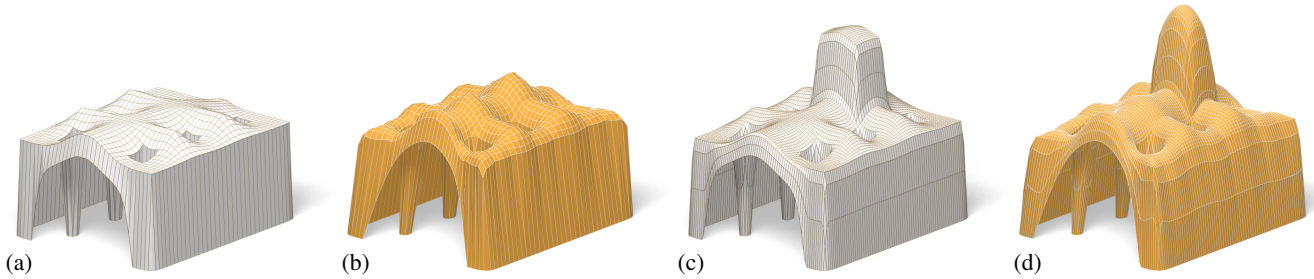


**Figure 6:** The user-designed reference mesh (a) is not self-supporting, but our algorithm finds a nearby perturbation of the reference surface (b) that is in equilibrium. As the user makes edits to the reference surface (c), the thrust network automatically adjusts (d).

equilibrium (6) and local integrability of  $\Phi$ . Doing so is equivalent to minimizing the squared residuals of Equations (3) and (2), with the positions held fixed. We define the *equilibrium energy*

$$E = \sum_i \left\| \begin{pmatrix} 0 \\ 0 \\ A_i F_i \end{pmatrix} - \sum_{j \sim i} w_{ij} (\mathbf{v}_j - \mathbf{v}_i) \right\|^2, \quad (7)$$

where  $i$  runs through interior and free boundary vertices, and solve

$$\min_{w_{ij}} E, \quad \text{s.t. } 0 \leq w_{ij} \leq w_{\max}. \quad (8)$$

Here  $w_{\max}$  is an optional maximum weight we are willing to assign (to limit the amount of stress in the surface). This convex, sparse, box-constrained least-squares problem [Friedlander 2007] always has a solution. If the objective is 0 at this solution, the faces of  $\Phi$  locally integrate to a stress surface satisfying (6), and this  $\Phi$  certifies that  $\mathcal{S}$  is self-supporting – we are done. Otherwise,  $\mathcal{S}$  is not self-supporting and its vertices must be moved.

**Step 3: Alter Positions.** In the previous step we fit as best as possible a stress surface  $\Phi$  to  $\mathcal{S}$ . There are two possible kinds of error with this fit: the faces around a vertex (equivalently, the reciprocal diagram) might not close up; and the resulting stress forces might not be exactly in equilibrium with the loads. These errors can be decreased by modifying the top view and heights of  $\mathcal{S}$ , respectively. It is possible to simply solve for new vertex positions that put  $\mathcal{S}$  in static equilibrium, since Equations (2) and (3) with  $w_{ij}$  fixed form a square linear system that is typically nonsingular.

While this approach would yield a self-supporting  $\mathcal{S}$ , this mesh is often far from the reference mesh  $\mathcal{R}$ , since any local errors in the stress surface from Step 2 amplify into global errors in  $\mathcal{S}$ . We propose instead to look for new positions that decrease the imbalance in the stresses and loads, while also penalizing drift away from the reference mesh:

$$\min_{\mathbf{v}} E + \alpha \sum_i \langle \mathbf{n}_i, \mathbf{v}_i - \mathbf{v}_i^0 \rangle^2 + \beta \|\mathbf{v} - \mathbf{v}_P^0\|^2,$$

where  $\mathbf{v}_i^0$  is the position of the  $i$ -th vertex at the start of this step of the optimization,  $\mathbf{n}_i$  is the starting vertex normal (computed as the average of the incident face normals),  $\mathbf{v}_P^0$  is the projection of  $\mathbf{v}^0$  onto the reference mesh, and  $\alpha > \beta$  are penalty coefficients that are decreased every iteration of Steps 1–3. The second term allows  $\mathcal{S}$  to slide over itself (if doing so improves equilibrium) but penalizes drift in the normal direction. The third term, weaker than the second, regularizes the optimization by preventing large drift away from the reference surface or excessive tangential sliding.

**Implementation Details.** Solving the weighted least-squares problem of Step 3 amounts to solving a sparse, symmetric linear system. While the MINRES algorithm [Paige and Saunders 1975] is likely the most robust algorithm for solving this system, in practice we have observed that the method of conjugate gradients works well despite the potential ill-conditioning of the objective matrix.



**Figure 7:** A freeform surface (left) needs adjustments around the entrance arch and between the two pillars in order to be self-supporting; our algorithm finds the nearby surface in equilibrium (right) that incorporates these changes.

Fig.	Vertices	Edges	Time (s)	Iterations	Max. Rel. Error
5b	1201	3504	21.6	9	$4.2 \times 10^{-5}$
5d	1200	3500	26.5	10	$8.5 \times 10^{-5}$
7	1535	2976	17.0	21	$2.7 \times 10^{-5}$
8	752	2165	8.0	9	$5.8 \times 10^{-5}$
11	2358	4302	19.5	9	$3.0 \times 10^{-4}$
16	527	998	5.7	25	$2.4 \times 10^{-5}$

**Table 1:** Numerical details about our examples. We show the clock time needed by an Intel Xeon 2.3GHz desktop PC with 4 GB of RAM to find a self-supporting thrust network and associated stress surface from the example’s reference mesh; we also give the number of outer iterations of the four steps in (§3). The maximum relative error is the dimensionless quantity  $\max_i \|A_i F_i - \sum_{j \sim i} w_{ij} (\mathbf{v}_j - \mathbf{v}_i)\| / \|A_i F_i\|$  (the maximum is taken over interior vertices  $\mathbf{v}_i$ ).

**Limitations.** This algorithm is not guaranteed to always converge; this fact is not surprising from the physics of the problem (if the boundary of the reference mesh encloses too large of a region,  $w_{\max}$  is set too low, and the density of the surface too high, a thrust network in equilibrium simply does not exist – the vault is too ambitious and cannot be built to stand; pillars are needed.)

We can, however, make a few remarks. Only Step 1 can increase the equilibrium energy  $E$  of Equation (7). Step 2 always decreases it, and Step 3 does as well as  $\beta \rightarrow 0$ . Moreover, as  $\alpha \rightarrow 0$  and  $\beta \rightarrow 0$ , Step 3 approaches a linear system with as many equations as unknowns; if this system has full rank, its solution sets  $E = 0$ . These facts suggest that the algorithm should generally converge to a thrust network in equilibrium, provided that Step 1 does not increase the loads by too much at every iteration, and this is indeed what we observe in practice. One case where this assumption is guaranteed to hold is if the thickness of the surface is allowed to freely vary, so that it can be chosen so that the surface has uniform density over the top view.

If the linear system in Step 3 is singular and infeasible, the algorithm can stall at  $E > 0$ . This failure occurs, for instance, when an interior vertex has height  $z_i$  lower than all of its neighbors, and

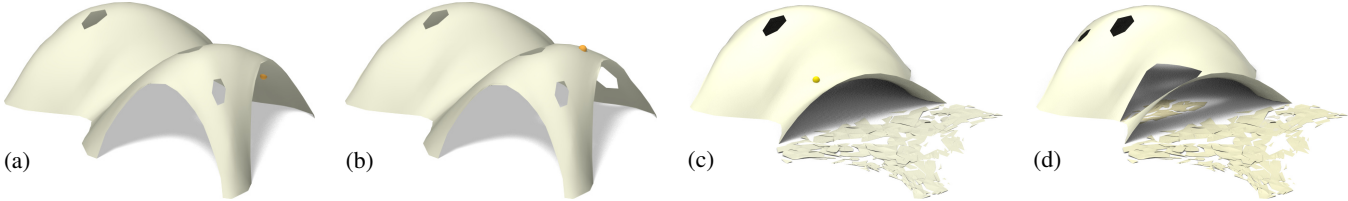


**Figure 8:** Destruction sequence. We simulate removing small parts of masonry (their location is shown by a yellow ball) and the falling off of further pieces which are no longer supported after removal. For this example, removing a certain small number of single bricks does not affect stability (a,b). Removal of material at a certain point (yellow ball in (b)) will cause a greater part of the structure to collapse, as seen in (c). (d) shows the result after one more removal (all images show the respective thrust networks, not the reference surface).

**Figure 9:** Stability Test. Left: Coloring and cross-section of edges visualize the magnitude of forces in a thrust network which is in equilibrium with this dome's dead load. Right: When an additional load is applied, there exists a corresponding compressive thrust network which is still contained in the masonry hull of the original dome. This implies stability of the dome under that load.

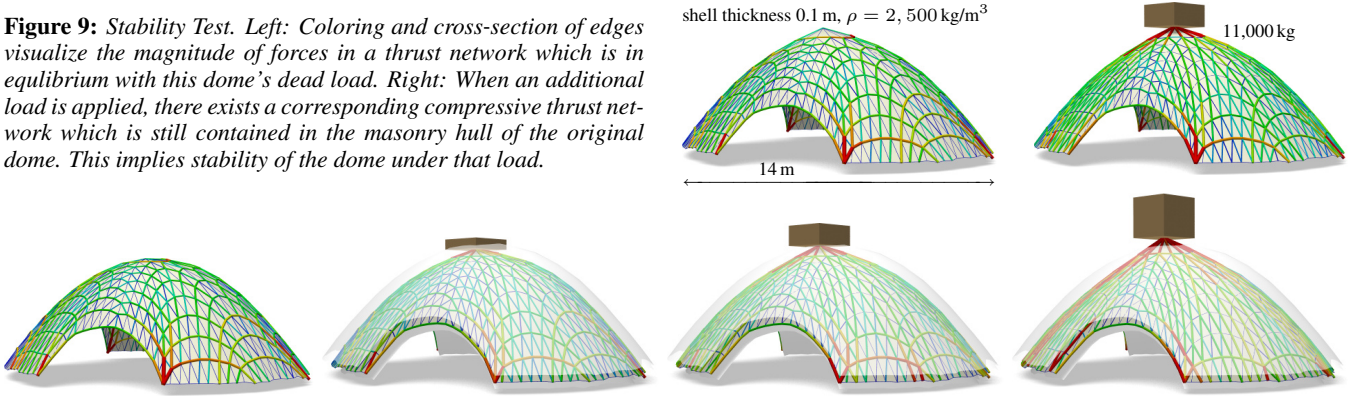


**Figure 10:** Stability test similar to Figure 9, but with a shell thickness of 1 m, in order to better visualize the way the thrust network starts to leave the masonry hull as the load increases. Additional loads are 0 kg, 5,000 kg, 10,000 kg, and 20,000 kg, resp., from left to right.

463 Step 2 assigns all incident edges to that vertex a weight of zero:  
 464 clearly no amount of moving the vertex or its neighbors can bring  
 465 the vertex into equilibrium. We avoid such degenerate configura-  
 466 tions by bounding weights slightly away from zero in (8), trading  
 467 increased robustness for slight smoothing of the resulting surface.  
 468 Attempting to optimize meshes that have self-intersecting top views  
 469 (i.e., aren't height fields), have too many impossible features, or are  
 470 insufficiently supported by fixed boundary points can also result in  
 471 errors and instability.

## 4 Results

473 **Interactive Design of Self-Supporting Surfaces.** The opti-  
 474 mization algorithm described in the previous section forms the ba-  
 475 sis of an interactive design tool for self-supporting surfaces. Users  
 476 manipulate a mesh representing a reference surface, and the com-  
 477 puter searches for a nearby thrust network in equilibrium (see e.g.  
 478 Figure 6). Features of the design tool include:

- 479 • Handle-based 3D editing of the reference mesh using Lapla-  
 480 cian coordinates [Lipman et al. 2004; Sorkine et al. 2003] to  
 481 extrude vaults, insert pillars, and apply other deformations to  
 482 the reference mesh. Handle-based adjustments of the heights,  
 483 keeping the top view fixed, and deformation of the top view,  
 484 keeping the heights fixed, are also supported. The thrust net-  
 485 work adjusts interactively to fit the deformed positions, giving  
 486 the usual visual feedback about the effects of edits on whether  
 487 or not the surface can stand.
- 488 • Specification of boundary conditions. Points of contact be-  
 489 tween the reference surface and the ground or environment  
 490 are specified by “pinning” vertices of the surface, specifying  
 491 that the thrust network must coincide with the reference mesh  
 492 at this point, and relaxing the condition that forces must be in

493 equilibrium there.

- 494 • Interactive adjustment of surface density  $\rho$ , external loads,  
 495 and maximum permissible stress per edge  $w_{\max}$ , with visual  
 496 feedback of how these parameters affect the fitted thrust net-  
 497 work.
- 498 • Upsampling of the thrust network through Catmull-Clark sub-  
 499 division and polishing of the resulting refined thrust network  
 500 using optimization (§3).
- 501 • Visualization of the stress surface dual to the thrust network  
 502 and corresponding reciprocal diagram.

503 **Examples. Vault with Pillars:** As an example of the design and  
 504 optimization workflow, consider a rectangular vault with six pillars,  
 505 free boundary conditions along one edge, fixed boundary condi-  
 506 tions along the others, and a tower extruded from the top of the sur-  
 507 face (see Figure 6). This surface is neither convex nor simply connected,  
 508 and exhibits a mix of boundary conditions, none of which cause  
 509 our algorithm any difficulty; it finds a self-supporting thrust net-  
 510 work near the designed reference mesh. The user is now free to  
 511 make edits to the reference mesh, and the thrust network adapts to  
 512 these edits, providing the user feedback on whether these designs  
 513 are physically realizable.

514 **Example: Top of the Lilium Tower.** Consider the top portion of the  
 515 steel-glass exterior surface of the Lilium Tower, which is currently  
 516 being built in Warsaw (see Figure 5). What if we had wanted to  
 517 build this surface out of masonry instead? This surface contains a  
 518 concave part with local minimum in its interior and so cannot pos-  
 519 sibly be self-supporting without modification. Given this surface as  
 520 a reference mesh, our algorithm constructs a nearby thrust network  
 521 in equilibrium without the impossible feature. The user can then  
 522 explore how editing the reference mesh – adding a pillar, for exam-  
 523 ple – affects the thrust network and its deviation from the reference  
 524 surface.

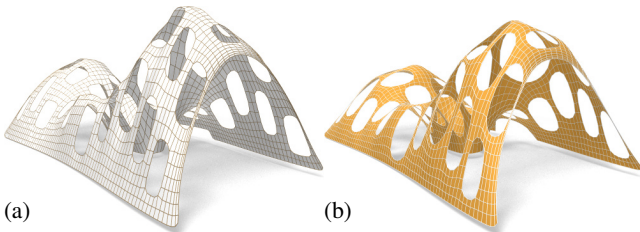


**Figure 11:** A mesh with holes (a) requires large deformations to both the top view and heights to render it self-supporting (b)

525 **Example: Freeform Structure with Two Pillars.** Suppose an architect's experience and intuition has permitted the design of a nearly  
526 self-supporting freeform surface (Figure 7). Our algorithm reveals  
527 those edits needed to make the structure sound – principally around  
528 the entrance arch, and the area between the two pillars.  
529

530 **Example: Destruction Sequence.** In Figure 8 we simulate removing  
531 parts of masonry and the falling off of further pieces which are no  
532 longer supported after removal. This is done by deleting the 1-  
533 neighborhood of a vertex and solving for a new thrust network in  
534 compressive equilibrium close to the original reference surface. We  
535 delete those parts of the network which deviate too much and are  
536 no longer contained in the masonry hull, and iterate.

537 **Example: Stability Test:** See Figures 9 and 10 for a series of images  
538 which visualize the effect of additional loads on a thrust network.

539 **Example: Swiss Cheese.** Cutting holes in a self-supporting surface  
540 interrupts force flow lines and causes dramatic global changes to  
541 the surface stresses, often to the point that the surface is no longer  
542 in equilibrium. Whether a given surface with many such holes can  
543 stand is far from obvious. Figure 11a shows such an implausible  
544 and unstable surface; our optimization finds a nearby, equally im-  
545 plausible but stable surface without difficulty (see Figures 1, left  
546 and 11b).

547 **Example: Structural Glass.** See Figure 16 for details on a self-  
548 supporting surface which is realized not as masonry, but as a steel/  
549 glass construction with glass as a structural element.

## 550 5 Special Self-Supporting Surfaces

551 **PQ Meshes.** Meshes with *planar* faces are of particular interest  
552 in architecture, so in this section we discuss how to remesh a given  
553 thrust network in equilibrium such that it becomes a quad mesh  
554 with planar faces (again in equilibrium). If this mesh is realized  
555 as a steel-glass construction, it is self-supporting in its beams alone,  
556 with no forces exerted on the glass (this is the usual manner of using  
557 glass). The beams constitute a self-supporting structure which is in

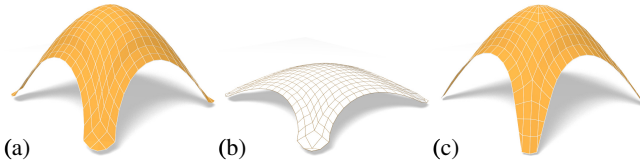


**Figure 12:** Directly enforcing planarity of the faces of even a very simple self-supporting quad-mesh vault (a) results in a surface far removed from the original design (b). Starting instead from a remeshing of the surface with edges following relative principal curvature directions yields a self-supporting, PQ mesh far more faithful to the original (c).

558 perfect force equilibrium (without moments in the nodes) if only  
559 the deadload is applied.

560 Taking an arbitrary non-planar quad mesh and attempting naive, si-  
561 multaneous enforcement of planarity and static equilibrium – either  
562 by staggering a planarity optimization step every outer iteration, or  
563 adding a planarity penalty term to the position update – does not  
564 yield good results, as shown in Figure 12. Indeed, as we will see  
565 later in this section, such a planar perturbation of a thrust network  
566 is not expected to generally exist.

567 Consider a planar quad mesh  $\mathcal{S}$  with vertices  $\mathbf{v}_{ij} = (x_{ij}, y_{ij}, s_{ij})$   
568 which approximates a given continuous surface  $s(x, y)$ . It is known  
569 that  $\mathcal{S}$  must approximately follow a network of conjugate curves in  
570 the surface (see e.g. [Liu et al. 2006]). We can derive this condition  
571 in an elementary way as follows: Using a Taylor expansion, we  
572 compute the volume of the convex hull of the quadrilateral  $\mathbf{v}_{ij}$ ,  
573  $\mathbf{v}_{i+1,j}$ ,  $\mathbf{v}_{i+1,j+1}$ ,  $\mathbf{v}_{i,j+1}$ , assuming the vertices lie exactly on the  
574 surface  $s(x, y)$ . This results in

$$\text{vol} = \frac{1}{6} \det(\mathbf{a}_1, \mathbf{a}_2) \cdot ((\mathbf{a}_1)^T \nabla^2 s \mathbf{a}_2) + \dots,$$

where  $\mathbf{a}_1 = \begin{pmatrix} x_{i+1,j} - x_{ij} \\ y_{i+1,j} - y_{ij} \end{pmatrix}$ ,  $\mathbf{a}_2 = \begin{pmatrix} x_{i,j+1} - x_{ij} \\ y_{i,j+1} - y_{ij} \end{pmatrix}$ ,

575 and the dots indicate higher order terms. We see that planarity re-  
576 quires  $(\mathbf{a}_1)^T \nabla^2 s \mathbf{a}_2 = 0$ . In addition to the mesh  $\mathcal{S}$  approximating  
577 the surface  $s(x, y)$ , the corresponding polyhedral Airy surface  $\Phi$   
578 must approximate  $\phi(x, y)$ ; thus we get the conditions

$$(\mathbf{a}_1)^T \nabla^2 s \mathbf{a}_2 = (\mathbf{a}_1)^T \nabla^2 \phi \mathbf{a}_2 = 0.$$

579  $\mathbf{a}_1, \mathbf{a}_2$  are therefore eigenvectors of  $(\nabla^2 \phi)^{-1} \nabla^2 s$ . In view of §2.3,  
580  $\mathbf{a}_1, \mathbf{a}_2$  indicate the principal directions of the surface  $s(x, y)$  rela-  
581 tive to  $\phi(x, y)$ .

582 In the discrete case, where  $s, \phi$  are not given as continuous surfaces,  
583 but are represented by a mesh in equilibrium and its Airy mesh, we  
584 use the techniques of Schiftner [2007] and Cohen-Steiner and Mor-  
585 van [2003] to approximate the Hessians  $\nabla^2 s, \nabla^2 \phi$ , compute prin-  
586 cipal directions as eigenvectors of  $(\nabla^2 \phi)^{-1} \nabla^2 s$ , and subsequently  
587 find meshes  $\mathcal{S}, \Phi$  approximating  $s, \phi$  which follow those directions.  
588 Global optimization can now polish  $\mathcal{S}, \Phi$  to a valid thrust network  
589 with discrete stress potential, where before it failed: we do so by  
590 taking the planarity energy  $\sum_f (2\pi - \theta_f)^2$ , where the sum runs  
591 over faces and  $\theta_f$  is the sum of the interior angles of face  $f$ , lin-  
592 earizing it at every iteration, and adding it to the objective function  
593 of the position update (Step 3). Convexity of  $\Phi$  ensures that  $\mathcal{S}$  is  
594 self-supporting.

595 Note that for each  $\Phi$ , the relative principal curvature directions give  
596 the *unique* curve network along which a planar quad discretization  
597 of a self-supporting surface is possible. Other networks lead to re-  
598 sults like the one shown by Figure 12. Figures 13 and 14 further  
599 illustrate the result of applying this procedure to self-supporting  
600 surfaces.

601 **Remark:** When remeshing a given shape by planar quad meshes, we  
602 know that the circular and conical properties require that the mesh  
603 follows the ordinary, Euclidean principal curvature directions [Liu  
604 et al. 2006]. It is remarkable that the self-supporting property in a  
605 similar manner requires us to follow certain *relative* principal direc-  
606 tions. Practitioners' observations regarding the beneficial statics  
607 properties of principal directions can be explained by this analogy,  
608 because the relative principal directions are close to the Euclidean  
609 ones, if the stress distribution is uniform and  $\|\nabla s\|$  is small.

610 **Koenigs Meshes.** Given a self-supporting thrust network  $\mathcal{S}$  with  
611 stress surface  $\Phi$ , we ask the question: Which vertical perturbation

**Figure 13:** Planar quad remeshing of the surface of Fig. 5. (a) Relative principal directions, found from eigenvectors of  $(\nabla^2\phi)^{-1}\nabla^2s$ . (b) Quad mesh guided by principal directions is almost planar and almost self-supporting. (c) Small changes achieve both properties.

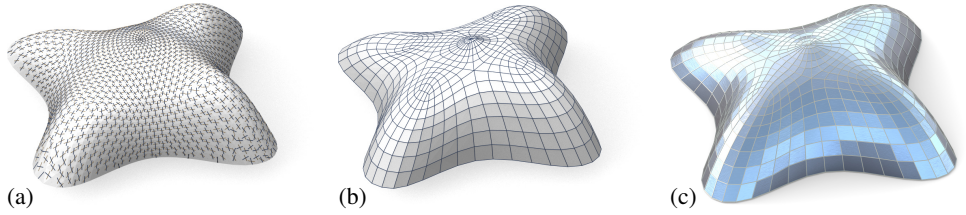


**Figure 14:** Planar quad remeshing of the surface of Figure 7. Left: Relative principal directions. Right: The result of optimization is a self-supporting PQ mesh, which guides a moment-free steel/glass construction (interior view, see also Fig. 1).



612  $\mathcal{S} + \mathcal{R}$  is self-supporting, with the same loads as  $\mathcal{S}$ ? As to notation,  
 613 all involved meshes  $\mathcal{S}, \mathcal{R}, \Phi$  have the same top view, and arithmetic  
 614 operations refer to the respective  $z$  coordinates  $s_i, r_i, \phi_i$  of vertices.

615 The condition of equal loads then is expressed as  $\Delta_\phi(s + r) =$   
 616  $\Delta_\phi s$  in terms of Laplacians or as  $H_{\mathcal{S}}^{\text{rel}} = H_{\mathcal{S} + \mathcal{R}}^{\text{rel}}$  in terms of mean  
 617 curvature, and is equivalent to

$$\Delta_\phi r = 0, \quad \text{i.e.,} \quad H_{\mathcal{R}}^{\text{rel}} = 0.$$

618 So  $\mathcal{R}$  is a *minimal surface* relative to  $\Phi$ . While in the triangle mesh  
 619 case there are enough degrees of freedom for nontrivial solutions,  
 620 the case of planar quad meshes is more intricate: Polar polyhedra  
 621  $\mathcal{R}^*, \Phi^*$  have to be Christoffel duals of each other [Pottmann and  
 622 Liu 2007], as illustrated by Figure 4. Unfortunately not all quad  
 623 meshes have such a dual; the condition is that the mesh is *Koenigs*,  
 624 i.e., the derived mesh formed by the intersection points of diagonals  
 625 of faces again has planar faces [Bobenko and Suris 2008].



**Figure 15:** A “Koebe” mesh  $\Phi$  is self-supporting for unit dead load. An entire family of self-supporting meshes with the same top view is defined by  $\mathcal{S}_\alpha = \Phi + \alpha\mathcal{R}$ , where  $\mathcal{R}$  is chosen as  $\Phi$ ’s Christoffel-dual.

626 **Koebe meshes.** An interesting special case occurs if  $\Phi$  is a  
 627 *Koebe mesh* of isotropic geometry, i.e., a PQ mesh whose edges  
 628 touch the Maxwell paraboloid. Since  $\Phi$  approximates the Maxwell  
 629 paraboloid, we get  $2K(\mathbf{v}_i)H^{\text{rel}}(\mathbf{v}_i) \approx 1$  and  $\Phi$  consequently is  
 630 self-supporting for unit load. Applying the Christoffel dual con-  
 631 struction described above yields a minimal mesh  $\mathcal{R}$  and a family of  
 632 meshes  $\Phi + \alpha\mathcal{R}$  which are self-supporting for unit load (see Fig-  
 633 ure 15).

## 6 Conclusion and Future Work

634 **Conclusion.** This paper builds on relations between statics and  
 635 geometry, some of which have been known for a long time, and  
 636 connects them with newer methods of discrete differential geom-  
 637 etry, such as discrete Laplace operators and curvatures of polyhedral

639 surfaces. We were able to find efficient ways of modeling self-  
 640 supporting freeform shapes, and provide architects and engineers  
 641 with an interactive tool for evaluating the statics of freeform  
 642 geometries. The self-supporting property of a shape is directly relevant  
 643 for freeform masonry. The actual thrust networks we use for  
 644 computation are relevant e.g. for steel constructions, where equilibrium  
 645 of deadload forces implies absence of moments. This theory  
 646 and accompanying algorithms thus constitute a new contribution to  
 647 architectural geometry, connecting statics and geometric design.

648 **Future Work.** There are several directions of future research. One  
 649 is to incorporate non-manifold meshes, which occur naturally when  
 650 e.g. supporting walls are introduced. It is also obvious that non-ver-  
 651 tical loads, e.g. wind load, play a role. There are also some direc-  
 652 tions to pursue in improving the algorithms, for instance adaptive  
 653 remeshing in problem areas. Probably the interesting connections  
 654 between statics and geometry are not yet exhausted, and we would  
 655 like to propose the *geometrization* of problems as a general solution  
 656 paradigm.

657 **Acknowledgements.** This work was very much inspired by  
 658 Philippe Block’s plenary lecture at the 2011 Symposium on Geom-  
 659 etry Processing in Lausanne. Several illustrations (the destruction  
 660 sequence of Figure 8 and the maximum load example of Figure 9)  
 661 have real-world analogues on his web page [Block 2011].

## References

- 663 ANDREU, A., GIL, L., AND ROCA, P. 2007. Computational anal-  
 664 ysis of masonry structures with a funicular model. *J. Engng.  
 665 Mechanics* 133, 473–480.
- 666 ASH, P., BOLKER, E., CRAPO, H., AND WHITELEY, W. 1988.  
 667 Convex polyhedra, Dirichlet tessellations, and spider webs. In  
 668 *Shaping space (Northampton 1984)*. Birkhäuser, 231–250.
- 669 BARNES, M. R. 2009. Form finding and analysis of tension struc-  
 670 tures by dynamic relaxation. *Int. J. Space Struct.* 14, 2, 89–104.
- 671 BLOCK, P., AND LACHAUER, L. 2011. Closest-fit, compression-  
 672 only solutions for free form shells. In *IABSE — IASS 2011 Lon-  
 673 don Symposium*, Int. Ass. Shell Spatial Structures. electronic.
- 674 BLOCK, P., AND OCHSENDORF, J. 2007. Thrust network analysis:  
 675 A new methodology for three-dimensional equilibrium. *J. Int.  
 676 Assoc. Shell and Spatial Structures* 48, 3, 167–173.

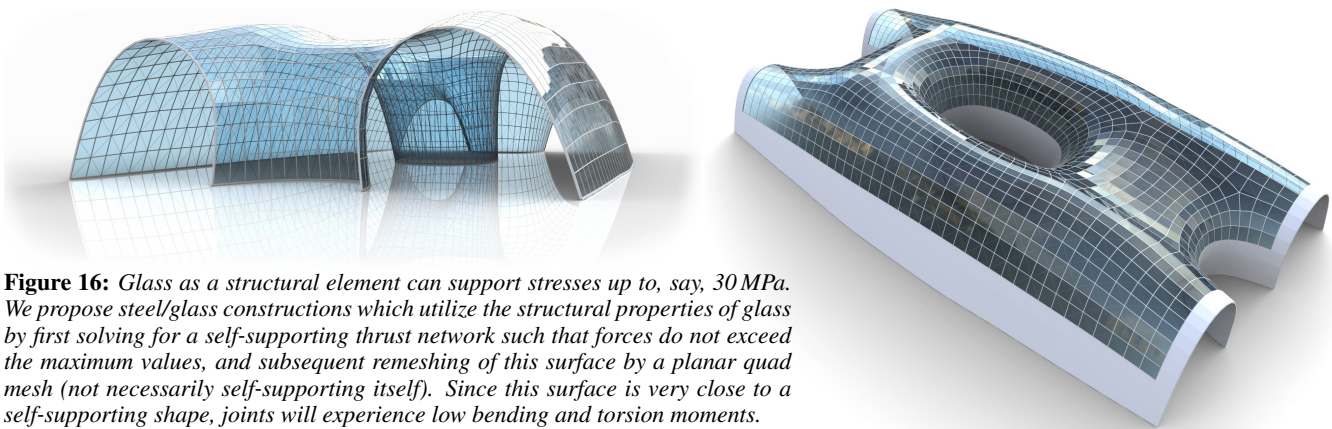


**Figure 16:** Glass as a structural element can support stresses up to, say, 30 MPa. We propose steel/glass constructions which utilize the structural properties of glass by first solving for a self-supporting thrust network such that forces do not exceed the maximum values, and subsequent remeshing of this surface by a planar quad mesh (not necessarily self-supporting itself). Since this surface is very close to a self-supporting shape, joints will experience low bending and torsion moments.

- 677 BLOCK, P. 2009. *Thrust Network Analysis: Exploring Three-dimensional Equilibrium*. PhD thesis, M.I.T.
- 678
- 679 BLOCK, P., 2011. Project webpage at <http://block.arch.ethz.ch/projects/freeform-catalan-thin-tile-vaulting>.
- 680
- 681 BOBENKO, A., AND SURIS, YU. 2008. *Discrete differential geometry: Integrable Structure*. American Math. Soc.
- 682
- 683 BOBENKO, A., POTTMANN, H., AND WALLNER, J. 2010. A curvature theory for discrete surfaces based on mesh parallelity. *Math. Annalen* 348, 1–24.
- 684
- 685 COHEN-STEINER, D., AND MORVAN, J.-M. 2003. Restricted Delaunay triangulations and normal cycle. In *Proc. 19th Symp. Computational Geometry*, ACM, 312–321.
- 686
- 687 FRATERNALI, F., ANGELILLO, M., AND FORTUNATO, A. 2002. A lumped stress method for plane elastic problems and the discrete-continuum approximation. *Int. J. Solids Struct.* 39,
- 688 6211–6240.
- 689
- 690 FRATERNALI, F. 2010. A thrust network approach to the equilibrium problem of unreinforced masonry vaults via polyhedral stress functions. *Mechanics Res. Comm.* 37, 2, 198 – 204.
- 691
- 692 FRIEDLANDER, M. P., 2007. BCLS: Bound constrained least squares. <http://www.cs.ubc.ca/~mpf/bcls>.
- 693
- 694 GIAQUINTA, M., AND GIUSTI, E. 1985. Researches on the equilibrium of masonry structures. *Archive for Rational Mechanics and Analysis* 88, 4, 359–392.
- 695
- 696 GLYMPH, J., SHELDEN, D., CECCATO, C., MUSSAL, J., AND SCHOBER, H. 2004. A parametric strategy for free-form glass structures using quadrilateral planar facets. *Automation in Construction* 13, 2, 187 – 202.
- 697
- 698 HEYMAN, J. 1966. The stone skeleton. *Int. J. Solids Structures* 2,
- 699 249–279.
- 700
- 701 HEYMAN, J. 1995. *The Stone Skeleton: Structural Engineering of Masonry Architecture*. Cambridge University Press.
- 702
- 703 HEYMAN, J. 1998. *Structural Analysis: A Historical Approach*. Cambridge University Press.
- 704
- 705 KILIAN, A., AND OCHSENDORF, J. 2005. Particle-spring systems for structural form finding. *J. Int. Assoc. Shell and Spatial Structures* 46, 77–84.
- 706
- 707 LIPMAN, Y., SORKINE, O., COHEN-OR, D., LEVIN, D., ROSSI, C., AND SEIDEL, H. 2004. Differential coordinates for interactive mesh editing. In *Proc. SMI*, IEEE, 181–190.
- 708
- 709
- 710
- 711
- 712
- 713
- 714
- 715
- 716
- 717 LIU, Y., POTTMANN, H., WALLNER, J., YANG, Y.-L., AND WANG, W. 2006. Geometric modeling with conical meshes and developable surfaces. *ACM Trans. Graphics* 25, 3, 681–689.
- 718
- 719 LIVESLEY, R. K. 1992. A computational model for the limit analysis of three-dimensional masonry structures. *Meccanica* 27, 161–172.
- 720
- 721 MAXWELL, J. 1864. On reciprocal diagrams and diagrams of forces. *Philosophical Magazine* 4, 27, 250–261.
- 722
- 723 O'Dwyer, D. 1998. Funicular analysis of masonry vaults. *Computers and Structures* 73, 187–197.
- 724
- 725 PAIGE, C. C., AND SAUNDERS, M. A. 1975. Solution of sparse indefinite systems of linear equations. *SIAM J. Num. Analysis* 12, 617–629.
- 726
- 727 POTTMANN, H., AND LIU, Y. 2007. Discrete surfaces in isotropic geometry. In *Mathematics of Surfaces XII*. Springer, 341–363.
- 728
- 729 POTTMANN, H., LIU, Y., WALLNER, J., BOBENKO, A., AND WANG, W. 2007. Geometry of multi-layer freeform structures for architecture. *ACM Trans. Graphics* 26, 3, #65,1–11.
- 730
- 731 SCHIFTNER, A., AND BALZER, J. 2010. Statics-sensitive layout of planar quadrilateral meshes. In *Advances in Architectural Geometry 2010*, C. Ceccato et al., Eds. Springer, Vienna, 221–236.
- 732
- 733 SCHIFTNER, A. 2007. *Planar quad meshes from relative principal curvature lines*. Master's thesis, TU Wien.
- 734
- 735 SORKINE, O., COHEN-OR, D., AND TOLEDO, S. 2003. High-pass quantization for mesh encoding. In *Symposium Geometry processing*. 42–51.
- 736
- 737 VAN MELE, T., AND BLOCK, P. 2011. A novel form finding method for fabric formwork for concrete shells. *J. Int. Assoc. Shell and Spatial Structures* 52, 217–224.
- 738
- 739 WÄCHTER, A., AND BIEGLER, L. T. 2006. On the implementation of a primal-dual interior point filter line search algorithm for large-scale nonlinear programming. *Math. Progr.* 106, 25–57.
- 740
- 741 WARDETZKY, M., MATHUR, S., KÄLBERER, F., AND GRINSPUN, E. 2007. Discrete Laplace operators: No free lunch. In *Symposium on Geometry Processing*. 33–37.
- 742
- 743 WHITING, E., OCHSENDORF, J., AND DURAND, F. 2009. Procedural modeling of structurally-sound masonry buildings. *ACM Trans. Graphics* 28, 5, #112,1–9.
- 744
- 745
- 746
- 747
- 748
- 749
- 750
- 751
- 752
- 753
- 754